Monthly Notices
of the
ROYAL ASTRONOMICAL SOCIETY

MNRAS **444,** 457–465 (2014) doi:10.1093/mnras/stu1351

Timing studies of X Persei and the discovery of its transient quasi-periodic oscillation feature

Z. Acuner,[1]★ S. Ç. İnam,[2] Ş. Şahiner,[1] M. M. Serim,[1] A. Baykal[1] and J. Swank[3]

[1]*Physics Department, Middle East Technical University, 06531 Ankara, Turkey*
[2]*Department of Electrical and Electronics Engineering, Başkent University, 06810 Ankara, Turkey*
[3]*Astrophysics Science Division, Goddard Space Flight Center, NASA, Greenbelt, MD 20771, USA*

Accepted 2014 July 3. Received 2014 July 2; in original form 2014 May 15

ABSTRACT

We present a timing analysis of X Persei (X Per) using observations made between 1998 and 2010 with the Proportional Counter Array (PCA) onboard the *Rossi X-ray Timing Explorer* (*RXTE*) and with the *INTEGRAL* Soft Gamma-Ray Imager (ISGRI). All pulse arrival times obtained from the *RXTE*-PCA observations are phase-connected and a timing solution is obtained using these arrival times. We update the long-term pulse frequency history of the source by measuring its pulse frequencies using *RXTE*-PCA and ISGRI data. From the *RXTE*-PCA data, the relation between the frequency derivative and X-ray flux suggests accretion via the companion's stellar wind. However, the detection of a transient quasi-periodic oscillation feature, peaking at ∼0.2 Hz, suggests the existence of an accretion disc. We find that double-break models fit the average power spectra well, which suggests that the source has at least two different accretion flow components dominating the overall flow. From the power spectrum of frequency derivatives, we measure a power-law index of ∼− 1, which implies that, on short time-scales, disc accretion dominates over noise, while on time-scales longer than the viscous time-scales, the noise dominates. From pulse profiles, we find a correlation between the pulse fraction and the count rate of the source.

Key words: accretion, accretion discs – stars: neutron – pulsars: individual: X Persei – X-rays: binaries.

1 INTRODUCTION

From *Ariel 5* and *Copernicus* observations, X Persei (X Per; 4U 0352+309) has been revealed as a persistent low-luminosity accreting pulsar with a pulse period of ∼836 s (White et al. 1976). The neutron star in the binary system has a wide orbit around a Be-type star with an orbital period of ∼250 d and an eccentricity of ∼0.11 (Delgado-Marti et al. 2001).

The binary orbit of the system is wide and rather circular, such that the X-ray pulsar does not pass through the equatorial disc of the Be star. Therefore, X Per does not exhibit Type I outbursts near periastron passages, despite the fact that such outbursts are typical of most Be X-ray binary systems. Taking into account the observed X-ray luminosities ($L_x \sim 10^{35}$ erg s^{-1}) of the system, Delgado-Marti et al. (2001) have suggested that accreting matter is supplied by a slow (∼150 km s^{-1}) and dense wind, possibly originating from the equatorial disc around the companion star.

The long-term pulse-period variation of the source has been monitored since the 1970s using observations from various X-ray observatories (Nagase 1989; Lutovinov et al. 1994; Haberl 1994; Robba et al. 1996; Di Salvo et al. 1998; Delgado-Marti et al. 2001; Lutovinov, Tsygankov & Chernyakova 2012). Before 1978, X Per was spinning up with a rate of $\dot{P}/P \sim -1.5 \times 10^{-4}$ yr^{-1}. Between 1978 and 2002, the source was in a long-term spin-down episode with a rate of $\dot{P}/P \sim 1.3 \times 10^{-4}$ yr^{-1}. After 2002, it was found that the spin rate changed sign again, as the source was found to spin up with a rate of $\dot{P}/P \sim -3.6 \times 10^{-4}$ yr^{-1}. This is significantly higher in magnitude compared to that of the previous spin-up episode before 1978.

In this paper, we present results of a timing analysis of X Per using observations from the Proportional Counter Array (PCA) onboard the *Rossi X-ray Timing Explorer* (*RXTE*) and from the *INTEGRAL* Soft Gamma-Ray Imager (ISGRI). In Section 2, we introduce the observations. In Section 3, we present our timing analysis. In Section 4, we summarize and discuss our results.

2 OBSERVATIONS

2.1 *Rossi X-ray Timing Explorer*

The PCA onboard the *RXTE* had five identical co-aligned proportional counter units (PCUs; Jahoda et al. 1996, 2006). Each PCU had an effective area of approximately 1300 cm^2. The PCA was able

★ E-mail: zeynepa@astroa.physics.metu.edu.tr

© 2014 The Authors
Published by Oxford University Press on behalf of the Royal Astronomical Society

Downloaded from https://academic.oup.com/mnras/article-abstract/444/1/457/1009862 by Middle East Technical University Library user on 24 July 2020

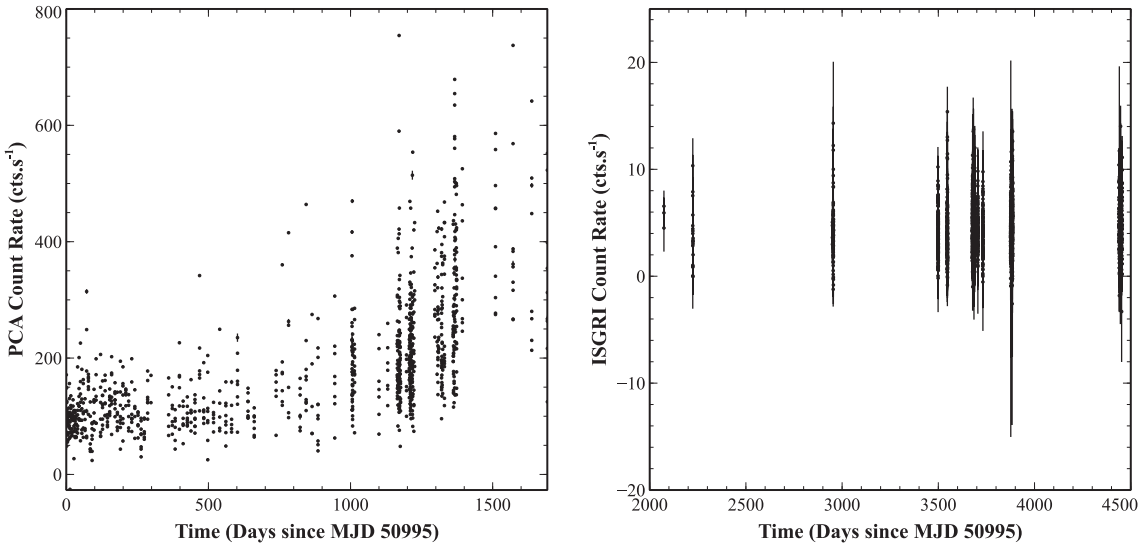


Figure 1. The 837-s binned light curves obtained from (left) *RXTE*-PCA (3–20 keV, corrected for five PCUs) and (right) *INTEGRAL* IBIS-ISGRI (20–40 keV) observations.

Table 1. List of *RXTE*-PCA observations.

Proposal ID	Exposure (ks)	Number of pointings	Time (MJD)
30099	252	56	50995–51406
40424	60	14	51420–51597
50404	58	12	51634–51940
60067	398	58	52000–52687
60068	25	8	52094–52398

to detect photons that had energies between 2 and 60 keV, with a spectral resolution of 18 per cent at 6 keV and a field of view (FOV) at full width at half-maximum (FWHM) of $\sim 1^\circ$. The number of active PCUs during the observations of X Per varied between one and three. Data from all the available PCUs are used in this analysis and the count rates shown in Fig. 1 are the values corrected as if five PCUs were operational.

X Per was observed by the *RXTE* between 1998 July 1 and 2003 February 17. The exposures of the individual pointed observations vary between 2 and 15 ks. The total exposure of 148 pointings adds up to ∼793 ks (see Table 1 for details). We extract light curves of the source with 0.1-s time binning in the 3–20 keV energy band using the `GoodXenon` mode events from the PCA.

The HEASOFT v.6.13 software is used for the PCA data analysis. Only the data corresponding to times when the elevation angle is greater than 10°, when the offset from the source is less than $0.^\circ02$ and when the electron contamination of PCU2 is less than 0.1 are analysed. The latest background estimator models supplied by the *RXTE* Guest Observer Facility are used to extract background spectra and light curves. These background subtracted light curves are corrected to the barycentre of the Solar system as well as for binary motion using the orbital parameters of X Per (see table 2 of Delgado-Marti et al. 2001).

2.2 *INTEGRAL*

The Imager onboard the *INTEGRAL* Satellite (IBIS) is a coded mask instrument optimized for high angular resolution (12 arcmin at FWHM; Ubertini et al. 2003). As a consequence of the large FOV ($8.^\circ3 \times 8.^\circ0$ fully coded, $29^\circ \times 29^\circ$ zero response) of IBIS observations and the dithering strategy of *INTEGRAL* observations, sky coverage is good and the exposure times of detected sources reach up to millions of seconds. The IBIS consists of two detector layers operating in different energy bands. The data analysed in this paper are obtained from the upper layer, the *INTEGRAL* Soft Gamma-Ray Imager (ISGRI), which operates in the energy range 15 keV–1 MeV, and has a time resolution of 61 μs.

When the offset of the source of interest increases, the coding factor decreases, resulting in increased uncertainties in the images, flux values and spectra. Therefore, it is not recommended to include in the analysis observations in which the source lies outside the 50 per cent partially coded FOV ($19^\circ \times 19^\circ$). Because X Per is a bright source, its flux is confidently determined even when its position is in the partially coded region. Consequently, the selection criteria for *INTEGRAL* observations are an off-axis angle of less than 10° and ISGRI good times of more than 1 ks. The publicly available pointing observations between MJD 53069 and 55451 (2004 March 5–2010 September 12) reach a number of 766 science windows (SCWs), each having typical durations of 2–3 ks. These observations have been analysed previously by Lutovinov et al. (2012), but in this paper we present a reanalysis of these observations in order to measure pulse periods using a different technique, as described in Section 3.1.

The latest version of the standard data analysis software OSA v.10.0 is used for pipeline processing. Images in two energy bands (20–40 and 40–60 keV) are generated from IBIS-ISGRI data with an input catalogue consisting of strong sources in the FOV: Crab, 3C 111, NGC 1275, IGR J02343+3229, XY Ari, 1H 0323+342, RX J0440.9+4431 and X Per. Background maps provided by the ISGRI team are used for background correction. The 10-s binned light curves are generated by the tool II_LIGHT and corrected to the Solar system barycentre. The effective exposure of the corrected IBIS-ISGRI light curve of X Per is around 2 Ms. The resulting light curves are also corrected for the binary motion using the orbital parameters of X Per (see Delgado-Marti et al. 2001).

Downloaded from https://academic.oup.com/mnras/article-abstract/444/1/457/1009862 by Middle East Technical University Library user on 24 July 2020

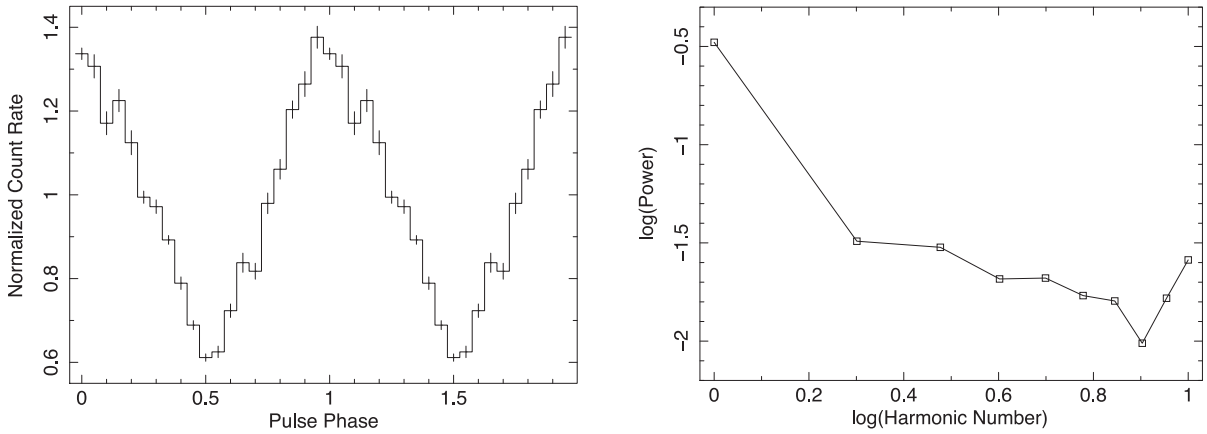


Figure 2. A typical pulse profile (left) obtained from *RXTE*-PCA and its power spectrum (right) in terms of harmonic number.

3 TIMING ANALYSIS

We use 0.1-s time binned *RXTE*-PCA and 10-s time binned *INTEGRAL* light curves, as described in Sections 2.1 and 2.2, for the timing analysis.

Fig. 1 presents overall 837-s binned *RXTE*-PCA and *INTEGRAL* light curves of the source.

3.1 Pulse timing

In order to measure the pulse periods of X Per, we fold time series on statistically independent trial periods (Leahy et al. 1983). We construct template pulse profiles by folding the data on the period corresponding to maximum χ^2. Pulse profiles consisting of 20 phase bins are represented by their Fourier harmonics (Deeter & Boynton 1985). Fig. 2 shows a typical pulse profile and the corresponding power spectrum in terms of harmonic number.

We have connected in phase all pulse arrival times of the *RXTE* observations over a 1550-d time-span. In the phase-connection process, we construct pulse arrival times for a time-span where the maximum phase shift is less than 1. In this way, we avoid cycle count ambiguity. This time-scale for X Per is around 220 d. We divide the total time-span into eight time intervals, each around 220 d. Then, we measure pulse arrival times with respect to the best period corresponding to that time interval. We align the slopes of the pulse arrival times in overlapping time intervals. The pulse arrival times thus measured are presented in the upper panel of Fig. 3.

In order to see the effect of pulse shape fluctuations, we estimate pulse arrival times using first, second, fifth and tenth harmonic numbers. Analysing each set in the same way, we obtain residuals consistent with each other within the 1σ level. Therefore, we conclude that pulse shape variations do not cause drastic changes in the pulse timing analysis.

The phase-connected pulse arrival times in Fig. 3 are fitted to the fifth-order polynomial,

$$\delta\phi = \delta\phi_{\rm o} + \delta\nu(t - t_0) + \sum_{n=2}^{5} \frac{1}{n!}\frac{{\rm d}^n\phi}{{\rm d}t^n}(t - t_0)^n \qquad (1)$$

where $\delta\phi$ is the pulse phase offset obtained from pulse timing analysis, t_0 is the mid-time of the observation, $\delta\phi_0$ is the residual phase offset at t_0, $\delta\nu$ is the correction of pulse frequency at time t_0 and ${\rm d}^n\phi/{\rm d}t^n$ for $n = 2$, 3, 4 and 5 are the first-, second-, third- and fourth-order derivatives of pulse frequency.

With only the statistical errors on the arrival phases, χ^2 per degree of freedom, which is 9.5, is not acceptable. Systematic errors or short-term variations not captured in the fifth-order polynomial could be responsible. The errors have been multiplied by a factor of 3 such that the reduced χ^2 is 1, in order to obtain errors on the polynomial fits to the longer-term variations. Pulse arrival times (pulse cycles) and the residuals of the fit after removal of the fifth-order polynomial trend are shown in Fig. 3. Table 2 presents the timing solutions for X Per between MJD 50995 and 52562.

In order to measure pulse frequencies, we fit a linear model to arrival times from ∼20–30 d intervals. The slopes of these linear fits give us estimates of the pulse frequency values at the mid-times of the corresponding intervals. Fig. 4 presents the resulting pulse periods of the source, together with the previous pulse period measurements of the source (see references in Lutovinov et al. 2012). In Fig. 4, we do not include measurements from *RXTE* and *INTEGRAL* by Lutovinov et al. (2012), because the values of their measurements are not reported numerically. However, when we

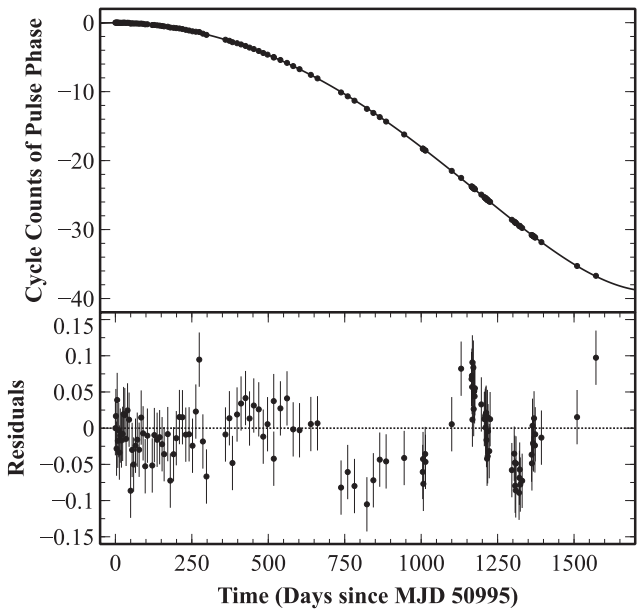


Figure 3. Pulse arrival times and their residuals after a fifth-order polynomial fit obtained from *RXTE*-PCA observations.

Downloaded from https://academic.oup.com/mnras/article-abstract/444/1/457/1009862 by Middle East Technical University Library user on 24 July 2020

Table 2. Timing solutions for X Per between MJD 50995 and 52562.

Parameter	Value
Epoch (t_0) (d, in MJD)	50995.038(1)
Timing parameters at t_0:	
Spin period (s)	837.666(6)
Spin frequency (Hz)	$1.19379(9) \times 10^{-3}$
$\dot{\nu}$ (Hz s^{-1})	$-5.5(3) \times 10^{-15}$
$\ddot{\nu}$ (Hz s^{-2})	$6.6(6) \times 10^{-23}$
$\dddot{\nu}$ (Hz s^{-3})	$-3.6(9) \times 10^{-30}$
$\ddddot{\nu}$ (Hz s^{-4})	$9(2) \times 10^{-38}$

compare the scanned values in fig. 2 of Lutovinov et al. (2012), it is seen that our measurements are in agreement with theirs. Table 3 presents our pulse period measurements.

For the timing analysis of *INTEGRAL* observations, we use 10-s binned background-corrected 20–40 keV IBIS-ISGRI light curves of the source. From the light curves that have ∼7–10 d time-spans, we measure the best pulse frequency by folding the light curve on statistically independent pulse frequencies. Then, we estimate the pulse arrival times by constructing master and sample pulses, as described above for the *RXTE* analysis. From the slopes of the pulse arrival times, $\delta\phi = \delta\nu(t - t_0)$, we obtain corrections to the pulse frequencies. In Fig. 4 and Table 3, we present pulse periods obtained from *INTEGRAL* observations.

We measure pulse frequency derivatives by fitting quadratic polynomials to ∼200-d long stretches of pulse arrival times from *RXTE*-PCA observations. The quadratic coefficients of the fits give the pulse frequency derivatives. The corresponding 3–20 keV X-ray flux values are calculated by modelling each corresponding spectrum with an absorbed blackbody and power-law model, a model previously used for this source (Lutovinov et al. 2012). In Fig. 5, we present the frequency derivatives and the corresponding flux measurements as a function of time, and the frequency derivative values as a function of unabsorbed 3–20 keV X-ray flux.

3.2 Broad excess and quasi-periodic oscillation features

We use the intensity power spectra obtained using `powspec` of HEASOFT from 0.3-s binned light curves of each *RXTE*-PCA observation in order to look for further periodicities, other than those caused by spin and orbital modulations. The power spectra usually exhibit a broad excess around ∼0.01–0.08 Hz and occasionally

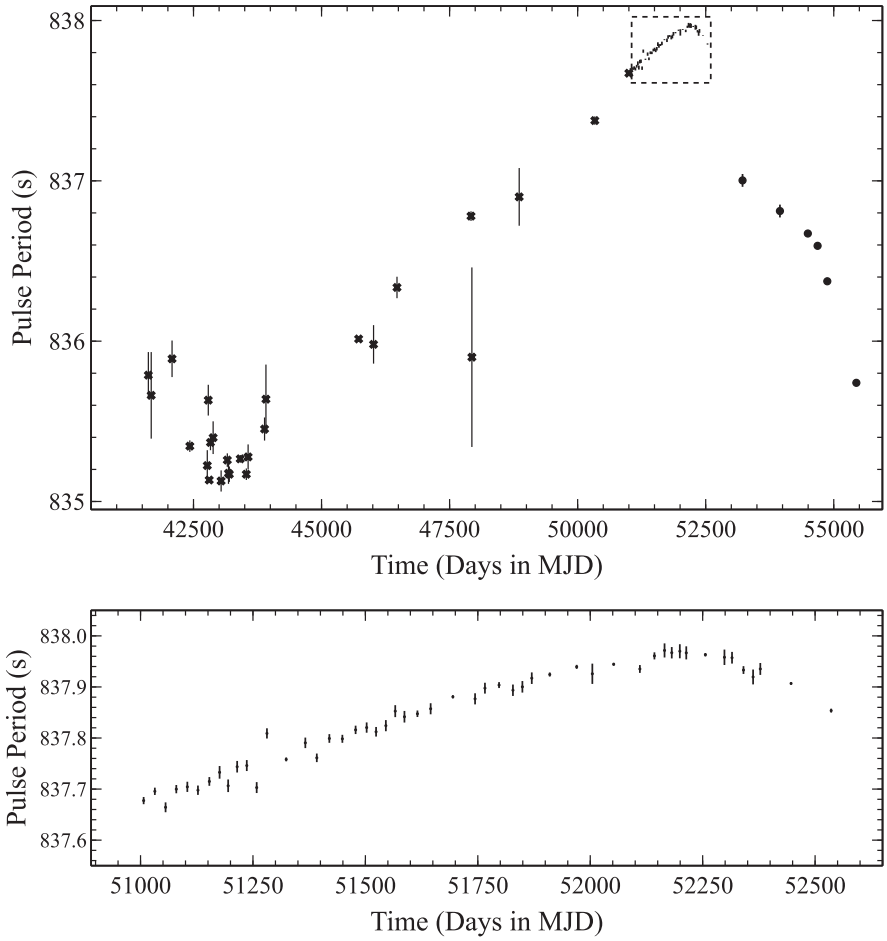


Figure 4. The top panel shows the pulse period history of X Per. Pulse periods denoted by crosses are previous measurements obtained from various observatories (see references in Lutovinov et al. 2012). The solid circles represent *INTEGRAL* measurements in this work. Other data points enclosed in the dashed rectangle are *RXTE*-PCA measurements of this work. The bottom panel shows a closer view of the pulse period evolution obtained from *RXTE*-PCA observations.

Downloaded from https://academic.oup.com/mnras/article-abstract/444/1/457/1009862 by Middle East Technical University Library user on 24 July 2020

Table 3. Pulse periods of X Per measured in this work. The numbers in parentheses indicate the uncertainties in the least significant figures.

Epoch (MJD)	Pulse period (s)	Epoch (MJD)	Pulse period (s)
51006.9	837.678(7)	51797.3	837.904(6)
51031.8	837.696(7)	51828.1	837.89(1)
51055.7	837.66(1)	51849.1	837.90(1)
51079.5	837.700(8)	51870.0	837.92(1)
51104.1	837.70(1)	51909.9	837.924(4)
51127.7	837.698(9)	51969.8	837.939(4)
51153.0	837.715(9)	52004.7	837.93(2)
51175.8	837.73(1)	52052.1	837.944(3)
51194.9	837.71(1)	52110.4	837.935(8)
51214.8	837.74(1)	52142.7	837.961(7)
51236.3	837.74(1)	52165.2	837.97(1)
51258.3	837.70(1)	52181.3	837.97(1)
51281.1	837.81(1)	52199.2	837.97(1)
51323.9	837.758(4)	52213.5	837.97(1)
51366.4	837.79(1)	52256.0	837.963(3)
51392.0	837.761(8)	52298.4	837.96(2)
51419.9	837.799(9)	52315.3	837.96(1)
51448.8	837.798(8)	52340.8	837.933(8)
51478.3	837.816(8)	52362.1	837.92(1)
51502.8	837.82(1)	52378.2	837.94(1)
51523.8	837.812(9)	52446.6	837.907(2)
51545.5	837.82(1)	52535.8	837.854(4)
51566.4	837.85(1)	53219.2[a]	837.00(4)
51586.9	837.84(1)	53949.3[a]	836.81(4)
51615.7	837.847(6)	54494.0[a]	836.67(2)
51645.1	837.86(1)	54684.5[a]	836.595(4)
51694.5	837.881(3)	54873.8[a]	836.37(2)
51743.9	837.88(1)	55441.1[a]	835.7402(3)
51765.9	837.90(1)		

[a] Pulse periods are measured from *INTEGRAL* observations.

exhibit a narrow excess peaking at ∼0.2 Hz, which can be interpreted as a transient quasi-periodic oscillation (QPO) feature.

In order to analyse the broad excess and the possible QPO features, all power spectra are fitted with a double power law. For the power spectra with a broad excess, a broad Gaussian is added to the model. Where a narrow excess is present, a Lorentzian is added to the model.

The broad excess feature appears between 0.01 and 0.02 Hz in the earlier observations and gradually shifts towards higher frequencies over time. This excess below 0.1 Hz can be observed in almost 90 per cent of the power spectra produced and it is mainly prominent between 0.02 and 0.08 Hz. Takeshima (1998) has previously found a 0.054-Hz QPO feature, in 1996 *RXTE* data, which lies in this frequency range. In our analysis of the later *RXTE* data, we find the activity in this range only as broad excess features, which are strong with high rms amplitudes, yet with coherence values too low to be considered QPOs.

In contrast, at around 0.2 Hz, we occasionally observe narrow peaks that can be interpreted as QPOs. For each observation, in order to test the significance of these QPOs, we average four power spectra and we rebin the frequencies by a factor of 4. Each resulting power spectrum is then normalized by dividing it by the continuum model consisting of a double power law and a broad Gaussian if a broad excess is present and multiplied by 2 (van der Klis 1989). The final power spectrum would be consistent with a χ^2 distribution for a degree of freedom $2 \times 4 \times 4 = 32$. According to this formalism, an excess power of 7 corresponds to a total power of $7 \times 4 \times 4 = 112$. The probability of detecting a false signal becomes $Q(112|32) = 8.2 \times 10^{-11}$. Because we have 128 independent frequencies in each power spectra, the total probability of having a false signal becomes $128 \times 8.2 \times 10^{-11} = 1.0 \times 10^{-8}$, which corresponds to more than a 5.73σ level of detection.

We find that only one of the QPOs peaking at ∼0.2 Hz has a significance at this level, which is the one at MJD 51060 (observation ID 30099-01-19-00). In Fig. 6, we present the intensity power spectrum and the power spectrum of this observation, normalized with respect to the continuum model. In the right panel of this figure, the 5.73σ level of detection is indicated as a horizontal dashed line,

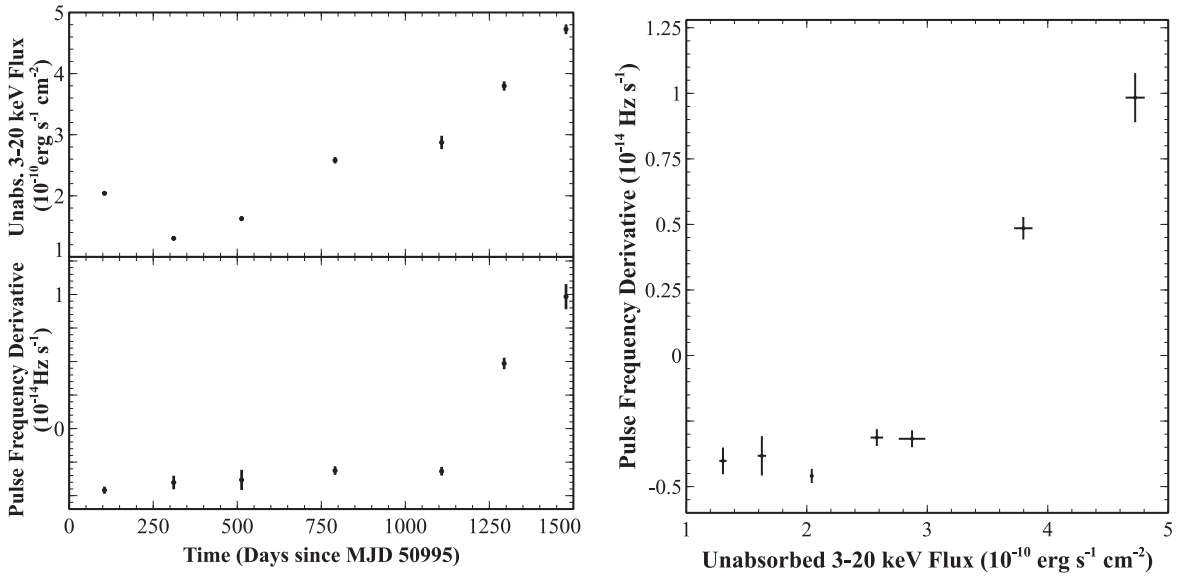


Figure 5. Left: unabsorbed 3–20 keV *RXTE*-PCA flux and frequency derivative as a function of time. Right: frequency derivative as a function of unabsorbed 3–20 keV *RXTE*-PCA flux.

Downloaded from https://academic.oup.com/mnras/article-abstract/444/1/457/1009862 by Middle East Technical University Library user on 24 July 2020

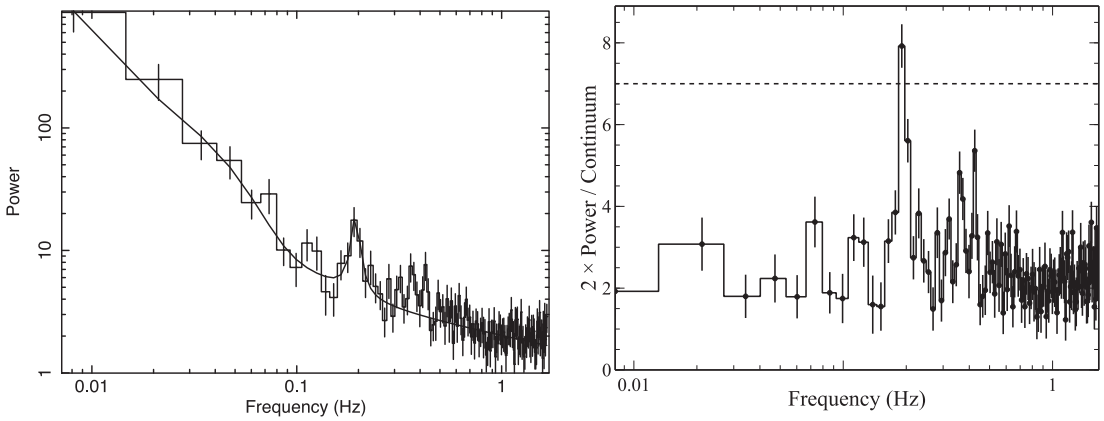


Figure 6. Left: power spectrum rebinned by a factor of 4 obtained from the *RXTE*-PCA observation ID 30099-01-19-00 (at MJD 51060). The QPO feature modelled as a Lorentzian peaked at 0.195 Hz is evident. Right: power spectrum rebinned by a factor of 4, multiplied by 2 and divided by the continuum modelled with a double power law with the addition of a broad Gaussian. Using the method of van der Klis (1989), a power value of 7 corresponds to a false signal probability of 1×10^{-8}, which is indicated as a horizontal dashed line.

and it is seen that there is only one feature above this level. For this observation, the continuum is modelled with a double power-law model with indices -0.36 ± 0.09 and -2.19 ± 0.30, with the addition of a Gaussian peaking at 0.016 Hz to account for the broad excess. The QPO is modelled as a Lorentzian peaked at 0.195 Hz with a width of 0.018 Hz. The QPO has a coherence (i.e. the peak frequency divided by the width) of 10.8 with an rms amplitude of 4.3 per cent, whereas the broad power excess has a coherence of 0.77 with an rms amplitude of 8.5 per cent.

In order to see the effect of time binning on power spectra, we rebin the light curve in 0.125 and 0.25 s, and reconstruct the power spectra. In all cases, QPO detections are found to have similar significance.

3.3 Average power spectra

Two power spectra are produced to examine the long-term averaged power spectral properties of X Per. Light curves obtained from observations with proposal ID 30099 (between MJD 50995 and 51406) and some of the observations with proposal ID 60067 (between MJD 52208 and 52687) are used to produce these two white-noise-subtracted power spectra using `powspec` of HEASOFT (see Fig. 7). Each average power spectrum is calculated by averaging the power spectra obtained from the *RXTE* light-curve portions in 1-s bins, each with a time-span of 4096 s. We avoid choosing larger time intervals because of the scarcity of data at the end of the *RXTE* observation time-span. It is convenient to pick out smaller time segments because they demonstrate the spectral behaviour of their broader counterparts. For both power spectra, the bin corresponding to the pulse frequency is replaced by the average of two neighbouring bins.

We find that a double-break power-law model fits these power spectra well. In this model, there are two breaks: the first break separates regions with f^0 (constant) and $f^{-1.4}$ dependence and the second break separates regions with $f^{-1.4}$ and f^{-2} dependence. For the first break, we find frequencies $7(2) \times 10^{-4}$ Hz and $9.3(8) \times 10^{-4}$ Hz for the first and second power spectra, respectively. For the second break, we find frequencies $2.3(2) \times 10^{-2}$ Hz and $2.36(9) \times 10^{-2}$ Hz for the two power spectra. Although the power spectra are found to be similar, the average unabsorbed 3–20 keV X-ray luminosities obtained from the energy spectra vary significantly, from $\sim 2.4 \times 10^{34}$ to 7×10^{34} erg s^{-1} for the first and second power spectra, respectively (assuming a source distance of 950 pc).

3.4 Power spectra of pulse frequency derivatives

In order to compare the torque fluctuations of X Per with other accreting X-ray pulsars, the power density spectrum for the pulse frequency variations is constructed. The red noise power density and associated random walk noise strengths are obtained using the technique developed by Deeter & Boynton (1982) and Deeter (1984). Some important properties are summarized here. For the rth-order red noise with strength S_r, the mean square residual for the data spanning an interval with length T is proportional to $S_r T^{2r-1}$.

The expected mean square residual, after removing a polynomial of degree m over an interval of length T, is given by

$$\langle \sigma_R^2(m, T) \rangle = S_r T^{2r-1} \langle \sigma_R^2(m, 1) \rangle_u, \quad (2)$$

where $\langle \sigma_R^2(m, 1) \rangle_u$ is the proportionality factor that can be estimated by measuring the variance of residuals by removing the degree of polynomial m for unit noise strength (S_1). We estimate this factor by simulating time series for the rth-order red noise process for a unit noise strength (S_1) for X Per observations. Our expected proportionality factors are consistent with those obtained by direct mathematical evaluation (Deeter 1984; see also Cordes 1980).

We obtain noise strengths at lower frequencies as $f = 1/T_{\rm max}$, where $T_{\rm max}$ is the maximum time-span of the pulse frequency history, from the residuals of pulse frequencies by removing their linear trends. For the higher frequencies, we have $f_n = n/T_{\rm max}$, where n is a positive integer and we remove quadratic trends from the pulse arrival times obtained from *RXTE* data.

In order to check whether noise strengths are stable or not, we estimate an alternative power spectra by removing quadratic trends in the pulse frequency at longer time-scales and cubic trends in pulse arrival times at shorter time intervals.

In Fig. 8, we present power spectra estimates (or noise strengths) with respect to frequency $f = n/T$ (or reciprocal of the time-scale). We find that both power spectra are consistent with each other in terms of the average noise strength S_r and the slope of the power spectra, -0.85 to -1.47, with a noise strength 10^{-20}–10^{-23} Hz s^{-2} for frequencies between 1/35 and 1 yr^{-1}.

Downloaded from https://academic.oup.com/mnras/article-abstract/444/1/457/1009862 by Middle East Technical University Library user on 24 July 2020

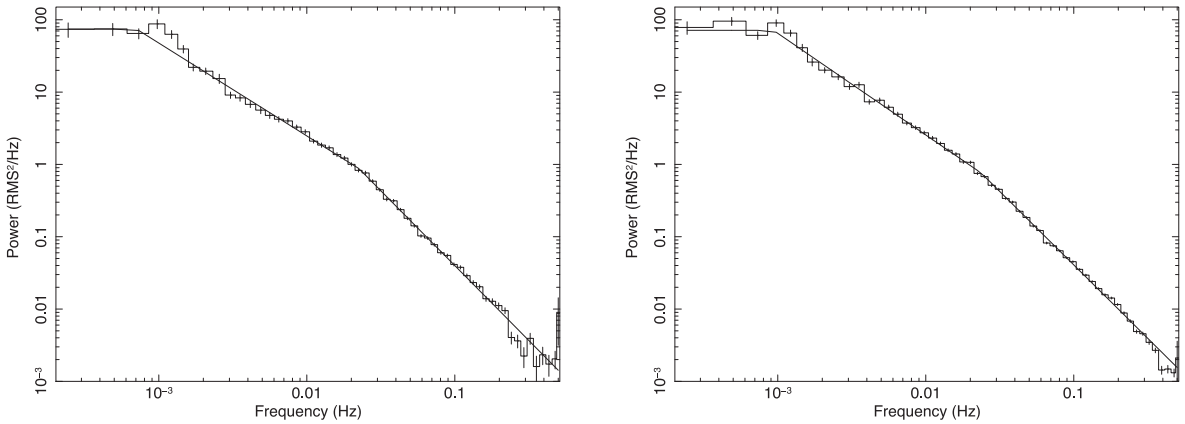


Figure 7. Average (summed) power spectra obtained from the *RXTE*-PCA observations (left) with proposal ID 30099 and (right) with proposal ID 60067. For each spectrum, the value of the bin that corresponds to the pulse frequency is removed by substituting it by the average of two neighbouring bins.

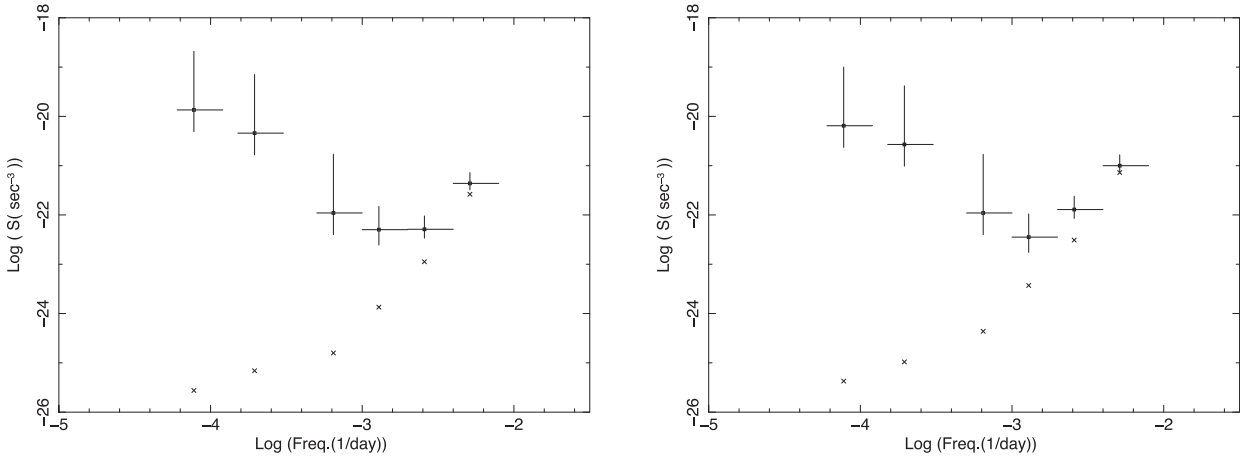


Figure 8. Power spectra estimated with respect to frequency obtained by removing (left) quadratic trends and (right) cubic trends. The crosses represent the power resulting from measurement noise.

3.5 Pulsed fraction

We investigate the pulsed fraction variation of X Per for all the available *RXTE*-PCA data between MJD 50995 and 52687 in the 3–20 keV energy band. Using the timing solution stated in Table 2, we extract 671 individual pulses of the source. Then we calculate the pulsed fraction and the mean count rate of each pulsation. The pulsed fractions are calculated with the standard definition,

$$\text{Pulsed fraction} = \frac{p_{\max} - p_{\min}}{p_{\max} + p_{\min}}, \tag{3}$$

where $p_{\min}$ and $p_{\max}$ refer to the minimum and maximum counts of the pulse, respectively. The pulsed fractions are then rebinned according to the mean count rate of the pulsations. The results indicate that the pulsed fraction of the source correlates with the mean count rate (see Fig. 9).

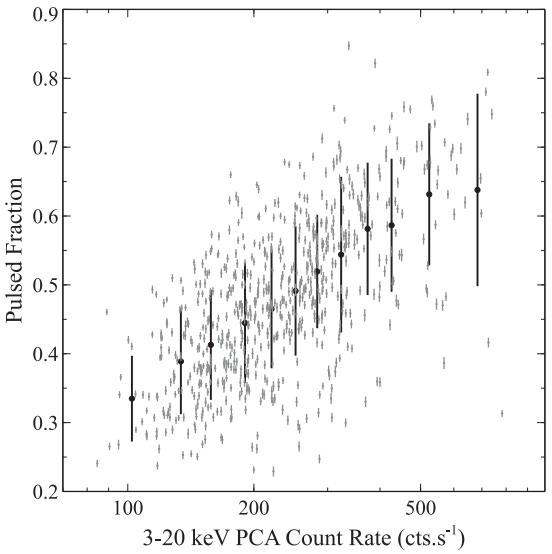


Figure 9. Variation of the pulsed fraction with the mean count rate of pulsations. The grey data points are the unbinned results, whereas the black data points are the results rebinned according to the count rates.

4 DISCUSSION

In this paper, we present our results of a timing analysis of *RXTE* and *INTEGRAL* observations of X Per. First, using the cross-correlation technique, we add new measurements to the pulse period history presented by Lutovinov et al. (2012); see Table 3.

From the right panel of Fig. 5, it is seen that the frequency derivative of the source correlates with the X-ray flux when the source

Downloaded from https://academic.oup.com/mnras/article-abstract/444/1/457/1009862 by Middle East Technical University Library user on 24 July 2020

spins up or down and the 3–20 keV X-ray flux is above $\sim 3 \times 10^{-10}$ erg s^{-1} cm^{-2}, while the frequency derivative does not vary significantly when source spins down and the 3–20 keV X-ray flux is below $\sim 3 \times 10^{-10}$ erg s^{-1} cm^{-2}. Fig. 5 resembles fig. 1 of Shakura et al. (2012), which presents the frequency derivative as a function of the normalized mass accretion rate (which should be positively correlated with the X-ray flux) of a neutron star accreting from a stellar wind. In fig. 1 of Shakura et al. (2012), a minimum spin-down rate value is reached when the mass accretion rate is equal to a critical mass accretion rate ($\dot{M}_{\rm cr}$) above which the spin rate is correlated with the mass accretion rate. Mass accretion rates below or above this value lead to smaller spin-down rates, and above a certain normalized mass accretion rate value (y_0), the source enters a spin-up regime. This similarity might indicate that the primary source of the accreted matter is the stellar quasi-spherical stellar wind of the companion. However, the transient QPO feature of the source suggests a transient formation of an accretion disc as the neutron star accretes via the companion's stellar wind. Another low-luminosity long-orbital-period persistent accretion-powered pulsar in a Be X-ray binary system, 1RXS J225352.8+624354, has recently been found to show signs of a possible transient accretion disc formation (Esposito et al. 2013).

QPOs with peak frequencies between 0.01 and 0.4 Hz have been observed in many accretion-powered pulsars (see İnam et al. 2004, and references therein). The QPO peak frequencies ($\sim$0.1–0.2 Hz) and rms amplitudes ($\sim$4 per cent) of X Per are typical.

Using a Keplerian frequency model (van der Klis et al. 1987), the QPO frequency is interpreted as the Keplerian frequency at the inner radius of the accretion disc. It can be expressed as

$$\nu_k = \frac{1}{2\pi}\left(\frac{GM}{r_0^3}\right)^{1/2}, \quad (4)$$

where M is the neutron star mass, which is taken as 1.4 M$_\odot$, r_0 is the radius of the inner disc and G is the universal gravitational constant. Using a Keplerian frequency model, we estimate the inner disc radius (r_0) as $\sim 4.99 \times 10^8$ cm for the most prominent QPO observed at MJD 51060 with a frequency of 0.192 Hz. It is important to note that because X Per's spin frequency is small compared to its QPO frequency, it is not observationally possible to discriminate between the Keplerian frequency model and the beat frequency model (Alpar & Shaham 1985).

The inner disc radius can also be expressed as (Ghosh & Lamb 1979)

$$r_0 \sim 0.52\mu^{4/7}(2GM)^{-1/7}\dot{M}^{-2/7}, \quad (5)$$

where $\mu = B \times R^3$ is the magnetic dipole moment, R is the neutron star radius, taken as 10^6 cm, and $\dot{M}$ is the mass accretion rate. At MJD 51060, when the most prominent QPO is observed, the 3–20 keV luminosity of the source is 4.38×10^{34} erg s^{-1}. This corresponds to a mass accretion rate of $\sim 2.4 \times 10^{14}$ g s^{-1}, assuming that this luminosity value is of the order of the bolometric luminosity and using the relation $L \simeq GM\dot{M}/R$. Then, the value of 3.56×10^{11} G is estimated for the surface dipole magnetic field of the source. This magnetic field estimate is roughly comparable to some previous magnetic field estimates ($\sim 2.5 \times 10^{12}$ G) of Lutovinov et al. (2012) and Coburn et al. (2001), based on the cyclotron resonance scattering feature in the energy spectra. However, our estimate is not consistent with the magnetar-like magnetic fields proposed for this source by Doroshenko et al. (2012).

The power spectra of pulse frequency derivatives have been studied for several accretion-powered X-ray pulsars. The random walk in pulse frequency or white noise in the pulse frequency derivative are suitable models for wind-accreting systems such as Vela X-1, 4U 1538-52 and GX 301-2 (Deeter 1981; Deeter et al. 1989; Bildsten et al. 1997). They have flat power spectra with white noise strengths in the range 10^{-20}–10^{-18} Hz s^{-2}. For 4U 1907+09, the random walk in pulse frequency is the appropriate model for frequencies between 1/1300 and 1/75 d^{-1} with noise strength 1.27×10^{-21} Hz s^{-2} (Şahiner, İnam & Baykal 2012). For 4U 1907+09, Şahiner et al. (2012) have suggested that at shorter time-scales there might be a transient accretion disc formation around the neutron star, which causes random walk in pulse frequency, while the source has a long-term steady spin-down trend. Her X-1 and 4U 1626-67 are disc accretors with low-mass companions. For these sources, it is found that pulse frequency time series are consistent with a random walk model with white noise strengths in the range 10^{-21}–10^{-18} Hz s^{-2}. However, red noise in the pulse frequency derivative cannot be excluded because of the sampling pulse frequencies and the narrow range of power spectra. The disc accretor Cen X-3 has red noise in its pulse frequency derivatives and the noise strength varies from low to high frequencies in the range 10^{-16}–10^{-18} Hz s^{-2} (Bildsten et al. 1997). The power-law index of the power spectra of X Per is ~ -1. This implies that at short time-scales, disc accretion dominates and noise is less; however, at longer time-scales greater than the viscous time-scales, there is excessive noise. The steepest power-law index for the power spectra of pulse frequency derivatives among high-mass X-ray binaries (HMXBs) has been seen in SAX J 2103.5+4545 with a power-law index of 2.13 (Baykal et al. 2007). For GX 1+4 and OAO 1657-415, the power-law indices ~ -1 and ~ 0, respectively, have been found. For these sources, accretion discs can be formed at short time-scales (Baykal 1997; Bildsten et al. 1997). X Per has the lowest noise strength (or torque noise) among the HMXBs discussed above (Baykal & Ögelman 1993; Bildsten et al. 1997). However, the steep power-law index or red noise in the pulse frequency derivative suggests that it could have a transient accretion disc.

From the two average (summed) power spectra obtained from 411-d and 479-d long observations (see Fig. 7), we find that a power-law model with two breaks, which correspond to transitions from the f^0 to $f^{-1.4}$ and $f^{-1.4}$ to f^{-2} parts of the power spectra, fits both power spectra well. These break frequencies are shown to be insensitive to the X-ray luminosity of the source, which might indicate that accretion geometry is not affected significantly as the accretion rate changes.

It is common to observe breaks in the power spectra of accretion-powered pulsars (see Revnivtsev et al. 2009, and references therein). Two breaks observed in the average power spectra of X Per might indicate that the source has at least two different accretion flow components dominating the overall flow. Sometimes, these breaks also correspond to different spectral states of sources if the power spectra are generated from data with a sufficiently long time interval (see İçdem & Baykal 2011).

The pulse fractions show a clear correlation with the source count rate. As the flux increases, the material appears to accrete more efficiently on the neutron star's magnetic poles. At higher mass accretion rates, the accreting plasma should be interacting with the magnetosphere closer to the neutron star. The shorter distance and the stronger field there could contribute to a higher fraction flowing to the poles.

ACKNOWLEDGMENTS

We acknowledge support from TÜBİTAK, the Scientific and Technological Research Council of Turkey through the research

Downloaded from https://academic.oup.com/mnras/article-abstract/444/1/457/1009862 by Middle East Technical University Library user on 24 July 2020

project TBAG 109T748. We thank Tod Strohmayer and Craig Markwardt for useful suggestions.

REFERENCES

Alpar M. A., Shaham J., 1985, Nat, 317, 681
Baykal A., 1997, A&A, 319, 515
Baykal A., Ögelman H., 1993, A&A, 267, 1
Baykal A., İnam S. Ç., Stark M. J., Heffner C. M., Erkoca A. E., Swank J. H., 2007, MNRAS, 374, 1108
Bildsten L. et al., 1997, ApJ, 113, 367
Coburn W., Heindl W. A., Gruber D., Rothschild R. E., Staubert R., Wilms J., Kreykenbohm I., 2001, ApJ, 552, 738
Cordes J. M., 1980, ApJ, 237, 216
Deeter J. E., 1981, PhD Thesis, Washington University
Deeter J. E., 1984, ApJ, 281, 482
Deeter J. E., Boynton P. E., 1982, ApJ, 261, 337
Deeter J. E., Boynton P. E., 1985, in Hayakawa S., Nagase F., eds, Proc. Inuyama Workshop: Timing Studies of X-Ray Sources. Nagoya Univ., Nagoya, p. 29
Deeter J. E., Boynton P. E., Lamb F. K., Zylstra G., 1989, ApJ, 336, 376
Delgado-Marti H., Levine A. M., Pfahl E., Rappaport S. A., 2001, ApJ, 546, 455
Di Salvo T., Burderi L., Robba N. R., Guainazzi M., 1998, ApJ, 509, 897
Doroshenko V., Santangelo A., Kreykenbohm I., Doroshenko R., 2012, A&A, 540, L1
Esposito P., Israel G. L., Sidoli L., Mason E., Rodriguez Castillo G. A., Halpern J. P., Moretti A., Gotz D., 2013, MNRAS, 433, 2028
Ghosh P., Lamb F., 1979, ApJ, 234, 296
Haberl F., 1994, A&A, 283, 175
İçdem B., Baykal A., 2011, A&A, 529, A7
İnam S. Ç., Baykal A., Swank J., Stark M. J., 2004, ApJ, 616, 463
Jahoda K., Swank J. H., Giles A. B., Stark M. J., Strohmayer T., Zhang W., Morgan E. H., 1996, Proc. SPIE, 2808, 59
Jahoda K., Markwardt C. B., Radeva Y., Rots A. H., Stark M. J., Swank J. H., Strohmayer T. E., Zhang W., 2006, ApJS, 163, 401
Leahy D. A., Darbro W., Elsner R. F., Weisskopf M. C., Kahn S., Sutherland P. G., Grindlay J. E., 1983, ApJ, 266, 160
Lutovinov A. A., Grebenev S. A., Sunyaev R. A., Pavlinsky M. N., 1994, Astron. Lett., 20, 538
Lutovinov A., Tsygankov S., Chernyakova M., 2012, MNRAS, 423, 1978
Nagase F., 1989, PASJ, 41, 1
Revnivtsev M., Churazov E., Postnov K., Tsygankov S., 2009, A&A, 507, 1211
Robba N. R., Burderi L., Wynn G. A., Warwick R. S., Murakami T., 1996, ApJ, 472, 341
Şahiner S., İnam S. Ç., Baykal A., 2012, MNRAS, 421, 2079
Shakura N., Postnov K., Kochetkova A., Hjalmarsdotter L., 2012, MNRAS, 420, 216
Takeshima T., 1998. in Katsuji K., Shunji K., Masayuki I., eds, Proc. IAU Symp. 188, The Hot Universe. Kluwer, Dordrecht, p. 368
Ubertini P. et al., 2003, A&A, 411, L131
van der Klis M., 1989, in Ögelman H., van den Heuvel E. P. J., eds, Timing Neutron Stars. Kluwer, Dordrecht, p. 27
van der Klis M., Stella L., White N., Jansen F., Parmar A. N., 1987, ApJ, 316, 411
White N. E., Mason K. E., Sanford P. W., Murdin P., 1976, MNRAS, 176, 20

This paper has been typeset from a TEX/LATEX file prepared by the author.

Downloaded from https://academic.oup.com/mnras/article-abstract/444/1/457/1009862 by Middle East Technical University Library user on 24 July 2020